derivatives (Table I). The assignments of the latter peaks are based on their characteristic numbers, frequency ranges, and relative intensities.[19] The infrared ν(CO) spectrum of (i-$Pr_2NP)_2P[Mn(CO)_5]Fe_2(CO)_6$ (IV) consists of only seven bands, which is not inconsistent with the observations that the E mode of the $Mn(CO)_5$ group remains unsplit, the B_1 mode is infrared inactive, and one of the weak A_1 modes of the $Mn(CO)_5$ group is obscured by the strong bands of the $Fe_2(CO)_6$ group around 1960 cm^{-1}. These infrared ν(CO) data suggest that the effective local symmetries of the ideal C_{3v} $Fe(CO)_4$ group in IX and the ideal C_{4v} $Cr(CO)_5$ groups in III and IV are considerably lowered by the effective local symmetry of the $Mn(CO)_5$ group in IV remains close to the ideal C_{4v}.

The phosphorus-31 NMR spectra of (i-$Pr_2NP)_2P(H)[Cr(CO)_5]Fe_2(CO)_6$ (VIII) and (i-$Pr_2NP)_2P(H)[Fe(CO)_4]Fe_2(CO)_6$ (IX) exhibit the following interesting features when compared with that of their precursors (i-$Pr_2NP)_2P(H)Fe_2(CO)_6$ (VI).

(1) Upon coordination the central phosphorus atoms of VIII and IX undergo only small chemical shift changes (19 ppm downfield for VIII and 5 ppm upfield for IX) whereas the terminal phosphorus atoms undergo much larger downfield chemical shifts (36 and 46 ppm for VIII and IX, respectively). The greater effect of the $Cr(CO)_5$ or $Fe(CO)_4$ group on the terminal phosphorus chemical shift rather than that of the center phosphorus to which it is directly bonded suggests that an effect of metal carbonyl complexation to the phosphorus lone pair in (i-$Pr_2NP)_2P(H)Fe_2(CO)_6$ (VI) is a change in the P-P-P bond angles involving the terminal phosphorus atoms. At the present time X-ray structural data are not available to test this idea.

(2) The one-bond $|^1J(P-H)|$ coupling constant of (i-$Pr_2NP)_2P(H)Fe_2(CO)_6$ (VI) increases as expected from 129 to 253 and 278 Hz for VIII and IX, respectively, whereas the two-bond $|^2J(P-H)|$ coupling constant of VI (8 Hz) decreases below the limits of detectability upon coordination of VI to $M(CO)_n$ groups to give VIII and IX, respectively.

Acknowledgment. We are indebted to the Air Force Office of Scientific Research for the partial support of this research at the University of Georgia under Grant AFOSR-84-0050.

Registry No. I, 101997-82-4; II (X = Cl), 101997-84-6; II (X = Br), 101997-85-7; II (X = OMe), 101997-86-8; II (X = OEt), 101997-87-9; II (X = H), 101997-88-0; III, 112863-59-9; IV, 112895-70-2; VII, 102046-52-6; VIII, 112895-69-9; IX, 112863-60-2; $Cr(CO)_6$, 13007-92-6; $Fe_2(CO)_9$, 15321-51-4; $Mn_2(CO)_{10}$, 10170-69-1; (i-$Pr_2NPH)_2PN(Pr$-$i)_2$, 101997-89-1; (i-$Pr_2NPH)_2PCl$, 102046-53-7.

Supplementary Material Available: Listings of positional parameters, anisotropic thermal parameters, and bond angles and distances for (i-$Pr_2NP)_2P(Cl)[Cr(CO)_5]Fe_2(CO)_6$ and (i-$Pr_2NP)_2P[Mn(CO)_5]Fe_2(CO)_6$ (11 pages); listings of observed and calculated structure factors (132 pages). Ordering information is given on any current masthead page.

(19) Braterman, P. S. *Metal Carbonyl Spectra*; Academic: London, 1975.

Contribution from the Departments of Chemistry, The University of Texas at Austin, Austin, Texas 78712, and University of Houston, Houston, Texas 77004

The Balance of Steric and Electronic Factors in Co_3 Cluster Geometry: Synthesis, Structure, Computations, and Electrochemistry of [Co(μ-Cy_2P)$(CO)_2]_3$ (Cy = Cyclohexyl)

Thomas A. Albright,*[1] Sung-Kwon Kang,[1] Atta M. Arif,[2] Allen J. Bard,*[2] Richard A. Jones,*[2,3] Jonathan K. Leland,†[2] and Stuart T. Schwab‡[2]

Received August 10, 1987

Reaction of $Co_2(CO)_8$ with Cy_2PH (Cy = cyclohexyl) (1/2) in toluene under reflux (8 h) yields [Co(μ-Cy_2P)$(CO)_2]_3$ (**1**) in 65% yield. The complex has been studied spectroscopically and electrochemically. The solid-state structure has been determined by X-ray diffraction and the electronic structure probed by extended Hückel molecular orbital calculations on the model complex [Co(μ-H_2P)$(CO)_2]_3$. Crystal data: $C_{40}H_{66}Co_3O_6P_3$, M_r = 912.69, monoclinic, $P2_1/a$ (No. 14), a = 18.912 (7) Å, b = 13.081 (5) Å, c = 20.253 (7) Å, β = 108.08 (3) Å, V = 4762.9 (5) Å^3, D_{calcd} = 1.273 g cm^{-3}, Z = 4, λ(Mo Kα) = 0.71073 Å (graphite monochromator), μ(Mo Kα) = 11.68 cm^{-1}. Methods: MULTAN, difference Fourier, full-matrix least squares. Refinement of 3788 reflections ($I > 3\sigma(I)$) out of 8992 unique observed reflections ($2° < 2\theta < 50°$) gave R and R_w values of 0.0710 and 0.0800, respectively. The data/parameter ratio = 7.471. The molecular structure of **1** consists of a Co_3 triangle with three edge-bridging Cy_2P^- units. Each Co atom bears two terminal CO ligands. There is considerable distortion of the structure from an idealized D_{3h} geometry. The three phosphido groups lie above, in, and below the Co_3 plane. In addition, each pair of terminal CO ligands adopts a configuration such that each C-Co-C plane is skewed from an orthogonal, idealized (D_{3h}) geometry. The overall geometry is roughly C_2. In solution, ^{31}P NMR spectra indicate a rapid fluxional motion that results in the phosphido ligands becoming equivalent. Extended Hückel calculations show that this cannot occur via a D_{3h} geometry. An analysis of possible reaction paths is given. The cyclic voltammetry of **1** in THF displays a reversible one-electron oxidation at 0.49 V (vs SCE), a reversible one-electron reduction (-0.96 V vs SCE), and a further quasi-reversible one-electron reduction (-1.56 V vs SCE) to give a dianion. The dianion of **1** can be generated chemically by reduction with Na/Hg in THF although the extreme air sensitivity of this brick red material has so far precluded its full characterization.

Introduction

Several di- and trinuclear diphenylphosphido (Ph_2P^-) bridged cobalt complexes have recently been described by Geoffroy and co-workers.[4] These complexes undergo some interesting dimer/trimer interconversions as well as ligand-exchange reactions. In contrast, the reaction of t-Bu_2PH with $Co_2(CO)_8$ produces the dinuclear Co=Co doubly bonded complex [Co(μ-t-Bu_2P)$(CO)_2]_2$, which appears to be relatively inert to reaction with CO or phosphines.[5] The large steric bulk of the t-Bu_2P groups is no doubt at least partially responsible for the lack of reactivity. In order to gain more insight into these systems, we investigated the reaction of Cy_2PH (Cy = cyclohexyl) with $Co_2(CO)_8$. If the differences in reactivity are due to steric factors, we expected to observe complexes of intermediate reactivity between those of Ph_2P^- and t-Bu_2P^- since Cy is not as large as t-Bu but considerably

†Present address: Igen Inc., Rockville, MD 20852.
‡Present address: Southwest Research Institute, San Antonio, TX 78284.

(1) University of Houston.
(2) The University of Texas at Austin.
(3) Alfred P. Sloan Fellow, 1985-1987.
(4) Harley, A. D.; Guskey, J. G.; Geoffroy, G. L. *Organometallics* **1983**, *2*, 53.
(5) Jones, R. A.; Stuart, A. L.; Atwood, J. L.; Hunter, W. E. *Organometallics* **1983**, *2*, 1437.

0020-1669/88/1327-1246$01.50/0

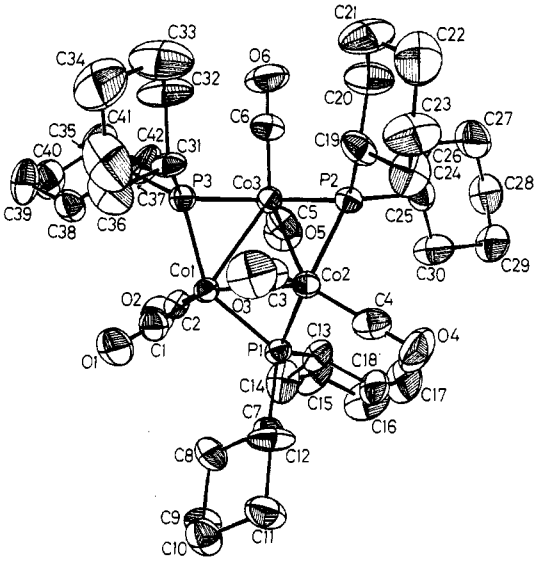

Figure 1. ORTEP view of $[Co(\mu\text{-}Cy_2P)_2(CO)_2]_3$ (**1**) with the atom-numbering scheme.

larger than Ph. Surprisingly, the reaction of $Co_2(CO)_8$ with 2 equiv of Cy_2PH in toluene under reflux produces the trimer $[Co(\mu\text{-}Cy_2P)(CO)_2]_3$ (**1**) in high yield. Although a number of phosphido-bridged cobalt carbonyl clusters are known,[4,6-8] only $[Co(\mu\text{-}Me_2P)(CO)_2]_3$[7] and $[Co(\mu\text{-}Ph_2P)(CO)_2]_3$,[8] together with **1**, have been structurally characterized. All three compounds in the solid state show severe distortions from idealized D_{3h} symmetries. In order to provide a rationale for these distortions, we have performed extended Hückel molecular orbital calculations on the model compound $[Co(\mu\text{-}H_2P)(CO)_2]_3$. We report here the synthesis, structure, and electrochemistry of **1**, as well as the results of our calculations.

Results and Discussion

Synthesis. Reaction of $Co_2(CO)_8$ with Cy_2PH (1/2) in toluene under reflux (8 h) gives a dark green solution from which $[Co(\mu\text{-}Cy_2P)(CO)_2]_3$ (**1**) can be isolated in 65% yield. **1** is a dark green, hexane-soluble, crystalline complex that is air stable both in the solid state and in solution for short periods. On the NMR time scale at room temperature, the three phosphido groups are chemically and magnetically equivalent, as are the CO ligands. Thus, the $^{13}C\{^1H\}$ NMR spectrum at 125.8 MHz has a single broad resonance at 209.7 ppm (relative to Me_4Si; $\Delta w_{1/2}$ = 29 Hz) at room temperature. The $^{31}P\{^1H\}$ NMR spectrum at 81.01 MHz consists of a single broad resonance (319.2 ppm relative to 85% H_3PO_4; $\Delta w_{1/2}$ = 80.6 Hz) at ambient temperature that is considerably broader at −90 °C ($\Delta w_{1/2}$ = 806.5 Hz). Broadening of the $^{31}P\{^1H\}$ NMR resonances in other dinuclear Co phosphido-bridged systems has been attributed to coupling to the ^{59}Co nucleus ($I = {}^7/_2$, 100%) since the signals *sharpened* as the temperature was lowered.[5,7] The broadening observed in the low-temperature $^{31}P\{^1H\}$ NMR spectrum of **1** is probably due to fluxional behavior that has not been frozen out into a low-temperature-limiting spectrum. This fluxionality, which gives a time-averaged solution structure of D_{3h} symmetry, has also been observed for $[Co(\mu\text{-}Me_2P)_2(CO)_2]_3$ by ^1H NMR spectroscopy.[7b] For this compound, exchange was rapid even at −90 °C; thus, the activation energy associated with this rearrangement must be quite small. A full discussion of the mechanism is deferred to the next section.

Despite the smaller size of the Cy_2P^- group vs that of $t\text{-}Bu_2P^-$, complex **1** does not display any increased reactivity compared to $[Co(\mu\text{-}t\text{-}Bu_2P)(CO)_2]_2$.[5] Thus, no reaction was observed between **1** and H_2, CO, C_2H_4, or CO_2 (3 atm). Nor could any reaction between **1** and PMe_3 be induced either thermally or photochemically (see Experimental Section). Reaction of **1** with an excess of sodium amalgam results in the formation of a sparingly soluble, highly air-sensitive brick red powder, which may be the dianion $[Co(\mu\text{-}Cy_2P)(CO)_2]_3^{2-}$. However, the low solubility and air sensitivity of this material precluded full characterization.

Structure and Dynamics of 1. **1** crystallizes from toluene at −20 °C in the monoclinic space group $P2_1/a$ with four molecules

Table I. Crystal Structure Parameters for $[Co(\mu\text{-}Cy_2P)(CO)_2]_3$ (**1**)

Description of Crystal	
color of cryst	green
habit of cryst	parallelepiped
max cryst dimens, mm	0.30 × 0.28 × 0.32
Unit Cell	
cryst system	monoclinic
space group	$P2_1/a$—special setting of No. 14
unit cell params	
a, Å	18.912 (7)
b, Å	13.081 (5)
c, Å	20.253 (7)
β, deg	108.08 (3)
V, Å^3	4762.9 (5)
Z	4
formula	$Co_3P_3O_6C_{40}H_{66}$
M_r	912.69
D_{calcd}, g cm^{-3}	1.273
μ_{calcd}, cm^{-1}	11.68
Data Collection	
radiation (λ, Å)	Mo Kα (0.71073)
scan technique	θ–2θ
scan width, deg	0.80 + 0.35 tan θ
range of indices (h,k,l)	+22,+15,±22
2θ range, deg	2–50
no. of reflcns measd	8992
Structure Determination	
no. of reflcns used ($I > 3\sigma(I)$)	3788
no. of params varied	507
shift to error ratio	3.189
esd of an observn of unit weight	5.1747
R^a	0.0710
R_w	0.0800

^{a} R and R_w are defined as $R = \sum||F_o| - |F_c|/\sum|F_o|$ and $R_w = [\sum w(|F_o| - |F_c|)^2/\sum w(|F_o|)^2]^{1/2}$.

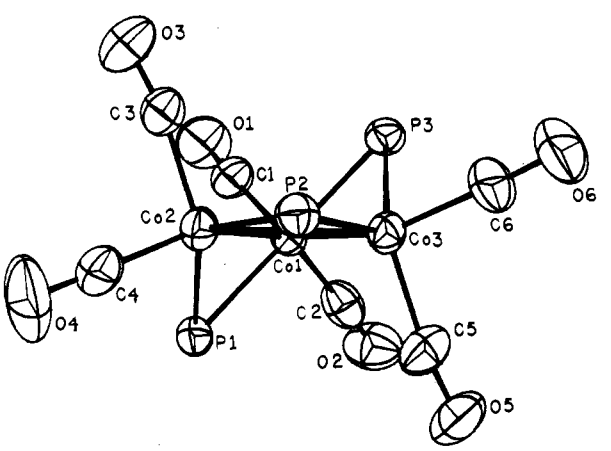

Figure 2. Side view of **1**. The cyclohexyl groups have been removed for clarity.

(6) (a) Vizi-Orosz, A.; Palyi, G.; Marko, L. *J. Organomet. Chem.* **1973**, *60*, C25. (b) Marko, L.; Marko, B. *Inorg. Chim. Acta* **1975**, *14*, L39. (c) Ryan, R. C.; Dahl, L. F. *J. Am. Chem. Soc.* **1975**, *97*, 6904. (d) Burt, J. C.; Boese, R.; Schmid *J. Chem. Soc., Dalton Trans.* **1978**, 1387. (e) Keller, E.; Vahrenkamp, H. *Chem. Ber.* **1979**, *112*, 1626. (f) Keller, E.; Vahrenkamp, H. *Angew. Chem., Int. Ed. Engl.* **1977**, *16*, 731. (g) Dobbie, R. J. C.; Whittaker, D. *J. Chem. Soc., Dalton Trans.* **1973**, 2427. (h) Hutching, L. D.; Light, R. W.; Paine, R. T. *Inorg. Chem.* **1982**, *21*, 266. (i) Grobe, J.; Stierand, H. *Z. Anorg. Allg. Chem.* **1969**, *371*, 99.
(7) (a) Keller, E.; Vahrenkamp, H. *J. Organomet. Chem.* **1978**, *155*, C41. (b) Keller, E.; Vahrenkamp, H. *Chem. Ber.* **1979**, *112*, 2347.
(8) Huntsman, J. R. Ph.D. Dissertation, University of Wisconsin, Madison, WI, 1973.

Table II. Positional Parameters for **1**[a,b]

atom	x	y	z	B, Å²
Co1	0.17025 (9)	0.1594 (1)	0.73483 (9)	2.65 (4)
Co2	0.04376 (9)	0.1793 (1)	0.75547 (9)	2.86 (4)
Co3	0.07982 (9)	0.0066 (1)	0.70185 (9)	2.81 (4)
P1	0.0856 (2)	0.2740 (3)	0.6876 (2)	2.84 (8)
P2	−0.0187 (2)	0.0382 (3)	0.7301 (2)	2.87 (7)
P3	0.1894 (2)	0.0048 (3)	0.7778 (2)	2.93 (7)
O1	0.2836 (6)	0.2609 (9)	0.8459 (6)	6.4 (3)
O2	0.2459 (6)	0.169 (1)	0.6312 (6)	6.1 (3)
O3	0.1077 (7)	0.188 (1)	0.9064 (5)	6.6 (3)
O4	−0.0807 (6)	0.311 (1)	0.7460 (7)	7.7 (4)
O5	0.0649 (6)	0.0266 (9)	0.5549 (5)	5.8 (3)
O6	0.0693 (7)	−0.2109 (8)	0.7063 (7)	6.7 (4)
C1	0.2370 (8)	0.224 (1)	0.8036 (7)	3.8 (3)
C2	0.2149 (7)	0.163 (1)	0.6720 (8)	4.0 (4)
C3	0.0869 (7)	0.177 (1)	0.8484 (7)	3.8 (3)
C4	−0.0305 (9)	0.258 (1)	0.7491 (7)	4.3 (4)
C5	0.0654 (8)	0.025 (1)	0.6112 (7)	4.5 (4)
C6	0.0739 (8)	−0.125 (1)	0.7030 (8)	4.4 (4)
C7	0.1068 (7)	0.412 (1)	0.7104 (7)	3.2 (3)
C8	0.1828 (8)	0.442 (1)	0.7025 (9)	5.0 (4)
C9	0.1993 (9)	0.558 (1)	0.7209 (9)	5.1 (4)
C10	0.1945 (9)	0.584 (1)	0.7921 (8)	5.0 (4)
C11	0.1173 (9)	0.554 (1)	0.7971 (9)	5.6 (4)
C12	0.103 (1)	0.436 (1)	0.7838 (8)	5.4 (4)
C13	0.0336 (8)	0.274 (1)	0.5914 (7)	4.0 (4)
C14	0.0828 (9)	0.307 (2)	0.5465 (7)	5.9 (5)
C15	0.037 (1)	0.288 (2)	0.4688 (8)	7.1 (5)
C16	−0.032 (1)	0.349 (2)	0.4508 (8)	8.0 (6)
C17	−0.082 (1)	0.325 (2)	0.496 (1)	8.0 (6)
C18	−0.0370 (8)	0.342 (1)	0.5765 (9)	5.5 (4)
C19	−0.0318 (7)	−0.020 (1)	0.8099 (7)	4.5 (4)
C20	−0.051 (1)	−0.134 (1)	0.8066 (8)	5.8 (5)
C21	−0.047 (1)	−0.169 (1)	0.8822 (9)	7.3 (5)
C22	−0.098 (1)	−0.106 (2)	0.9115 (9)	7.8 (6)
C23	−0.084 (1)	0.009 (2)	0.9095 (8)	7.0 (5)
C24	−0.0841 (9)	0.043 (2)	0.8369 (7)	5.7 (4)
C25	−0.1127 (8)	0.025 (1)	0.6614 (8)	4.4 (4)
C26	−0.1165 (9)	−0.076 (1)	0.6239 (8)	4.9 (4)
C27	−0.196 (1)	−0.089 (2)	0.569 (1)	7.0 (5)
C28	−0.2122 (9)	0.001 (2)	0.5207 (8)	5.6 (4)
C29	−0.2080 (9)	0.105 (1)	0.5581 (8)	5.3 (4)
C30	−0.127 (1)	0.115 (1)	0.6137 (9)	5.9 (5)
C31	0.1972 (8)	−0.024 (1)	0.8694 (6)	3.5 (3)
C32	0.194 (1)	−0.140 (1)	0.8830 (8)	6.7 (5)
C33	0.191 (1)	−0.159 (2)	0.9579 (9)	8.7 (6)
C34	0.259 (1)	−0.113 (2)	1.012 (1)	8.9 (7)
C35	0.259 (1)	0.004 (2)	0.9977 (9)	8.8 (6)
C36	0.266 (1)	0.025 (2)	0.9234 (7)	6.1 (5)
C37	0.2640 (8)	−0.073 (1)	0.7594 (7)	3.5 (3)
C38	0.3383 (8)	−0.013 (1)	0.7817 (8)	4.6 (4)
C39	0.4007 (8)	−0.077 (2)	0.7665 (9)	6.2 (5)
C40	0.3802 (9)	−0.104 (2)	0.689 (1)	6.4 (5)
C41	0.306 (1)	−0.162 (2)	0.667 (1)	6.9 (5)
C42	0.2423 (9)	−0.104 (1)	0.6815 (8)	5.4 (4)

[a] Anisotropically refined atoms are given in the form of the isotropic equivalent thermal parameter defined as $^4/_3[a^2B(1,1) + b^2B(2,2) + c^2B(3,3) + ab(\cos\gamma)B(1,2) + c(\cos\beta)B(1,3) + bc(\cos\alpha)B(2,3)]$. [b] Numbers in parentheses are estimated standard deviations in the least significant digits.

in the unit cell. Details of the X-ray structure determination are given in the Experimental Section and also in Table I. Positional parameters and selected bond lengths and angles are given in Tables II–IV, respectively. A view of the molecule projecting onto the Co_3 plane is shown in Figure 1. A side view of the molecule is shown in Figure 2. Here the Co_3 plane is roughly perpendicular to the plane of the paper, and the cyclohexyl groups have been omitted for clarity. Clearly, two phosphido groups, P1 and P3, lie below and above the plane defined by the three Co atoms, whereas P2 lies essentially in this plane. The dihedral angles between the Co1–Co2–Co3 plane and the bridging phosphides are 60.7° (Co1–P1–Co2), 60.6° (Co1–P3–Co3), and 4.4° (Co2–P2–Co3). There is a more irregular pattern in $[Co(\mu\text{-}Me_2P)_2(CO)_2]_3$,[7] where the corresponding dihedral angles are 70, 43, and 24°. In **1**, there is essentially a C_2 axis that passes through

Table III. Selected Bond Distances (Å) for **1**[a]

Co1–Co2	2.566 (3)	Co3–C6	1.72 (1)
Co1–Co3	2.580 (2)	P1–C7	1.87 (1)
Co1–P1	2.185 (4)	P1–C13	1.89 (1)
Co1–P3	2.187 (4)	P2–C19	1.87 (2)
Co1–C1	1.775 (13)	P2–C25	1.895 (13)
Co1–C2	1.73 (2)	P3–C31	1.85 (1)
Co2–Co3	2.685 (3)	P3–C37	1.87 (2)
Co2–P1	2.173 (4)	O1–C1	1.13 (2)
Co2–P2	2.165 (4)	O2–C2	1.15 (2)
Co2–C3	1.805 (12)	O3–C3	1.13 (2)
Co2–C4	1.72 (2)	O4–C4	1.16 (2)
Co3–P2	2.153 (4)	O5–C5	1.14 (2)
Co3–P3	2.164 (3)	O6–C6	1.13 (2)
Co3–C5	1.786 (15)		

[a] Numbers in parentheses are estimated standard deviations in the least significant digits.

Table IV. Selected Bond Angles (deg) for **1**[a]

Co2–Co1–Co3	62.90 (7)	P2–Co3–P3	122.0 (2)
Co2–Co1–P1	53.7 (1)	P2–Co3–C5	112.3 (5)
Co2–Co1–P3	94.4 (1)	P2–Co3–C6	97.1 (6)
Co2–Co1–C1	107.2 (5)	P3–Co3–C5	122.6 (5)
Co2–Co1–C2	144.0 (4)	P3–Co3–C6	91.8 (5)
Co3–Co1–P1	94.7 (1)	C5–Co3–C6	99.0 (8)
Co3–Co1–P3	53.2 (1)	Co1–P1–Co2	72.2 (1)
Co3–Co1–C1	145.5 (5)	Co1–P1–C7	118.7 (4)
Co3–Co1–C2	105.2 (5)	Co1–P1–C13	121.9 (5)
P1–Co1–P3	144.8 (2)	Co2–P1–C7	119.0 (5)
P1–Co1–C1	105.3 (5)	Co2–P1–C13	118.6 (5)
P1–Co1–C2	96.9 (5)	C7–P1–C13	104.7 (6)
P3–Co1–C1	97.9 (5)	Co2–P2–Co3	76.9 (1)
P3–Co1–C2	104.8 (5)	Co2–P2–C19	110.6 (5)
C1–Co1–C2	100.1 (7)	Co2–P2–C25	124.7 (5)
Co1–Co2–Co3	58.80 (7)	Co3–P2–C19	120.5 (5)
Co1–Co2–P1	54.1 (1)	Co3–P2–C25	118.7 (6)
Co1–Co2–P2	110.0 (1)	C19–P2–C25	104.6 (7)
Co1–Co2–C3	91.5 (5)	Co1–P3–Co3	72.7 (1)
Co1–Co2–C4	146.2 (6)	Co1–P3–C31	122.7 (5)
Co3–Co2–P1	92.0 (1)	Co1–P3–C37	117.7 (5)
Co3–Co2–P2	51.3 (1)	Co3–P3–C31	118.3 (5)
Co3–Co2–C3	108.6 (5)	Co3–P3–C37	118.7 (4)
Co3–Co2–C4	141.4 (5)	Co1–Co3–Co2	58.30 (7)

[a] Numbers in parentheses are estimated standard deviations in the least significant digits.

P2 and Co1. The coordination geometry around each Co atom can be described as roughly octahedral. The molecule has 48 valence electrons associated with the metals and is saturated with the formulation of three Co–Co single bonds. The average Co–Co bond length is 2.610 Å, which is in the range of other Co–Co single bonds.[9] The metal–metal bond bridged by the "in-plane" phosphido group is significantly longer (ca. 0.11 Å) than the other two metal–metal bonds. Extended Hückel calculations (vide infra) indicate that there is no decisive electronic driving force for this pattern. Elongating the two shorter Co–Co bonds to 2.685 Å from the experimental structure required only 1.6 kcal/mol. This is also consistent with the structure of $[Co(\mu\text{-}Me_2P)_2(CO)_2]_3$. Here the Co–Co bond lengths range from 2.514 (2) to 2.673 (2) Å, and there is no clear relationship between these bond lengths and the folding of the phosphido groups out of the Co_3 plane.[7]

With 48 valence electrons, the structures of the $[Co(\mu\text{-}R_2P)_2(CO)_2]_3$ series should be related to the prototype $Os_3(CO)_{12}$ or $Ru_3(CO)_{12}$ structure shown at the top of Scheme I. There are in fact three stereochemical ways to bridge the phosphido groups. **2**–**4** illustrate the resulting structures when two carbonyl groups at each metal are replaced by phosphido groups and the positions of the remaining carbonyls are not altered from the $M_3(CO)_{12}$ model. The observed structure in the solid state, **5**, is related rather simply to **2** by twisting the $Co(CO)_2$ group at Co1 by 47.9°. As mentioned previously, this gives an octahedral

(9) Bonding interactions have been observed in Co_3 species up to 2.687 (3) Å. See: Frisch, D. P.; Dahl, L. F. *J. Am. Chem. Soc.* **1972**, *94*, 5082.

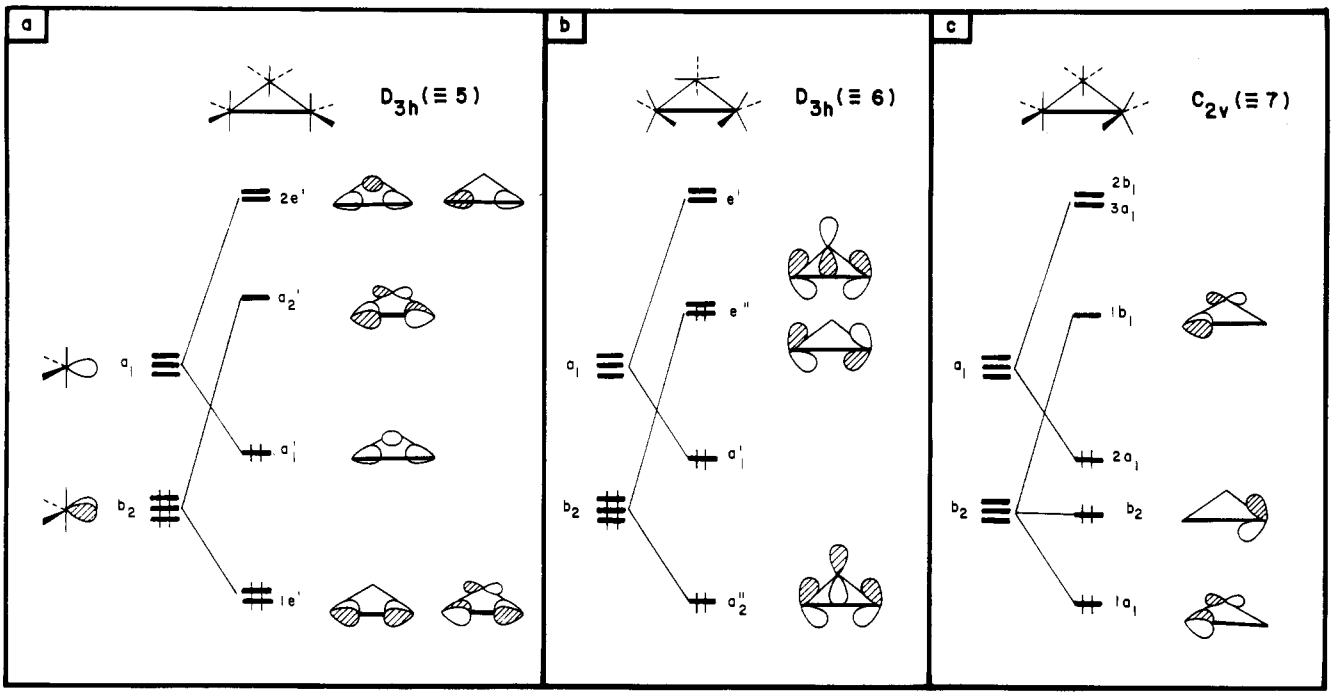

Figure 3. Building the M–M bonding in three structures for a 48-electron M_3L_{12} cluster.

Scheme I

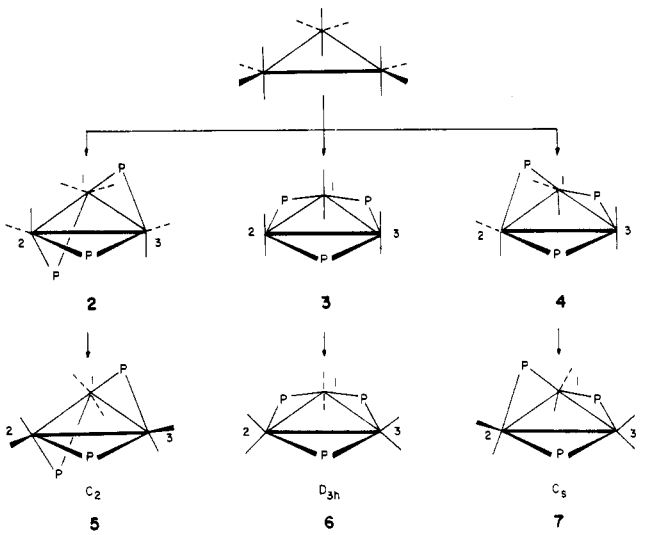

geometry at Co1. The two phosphido groups that bridge Co1–Co2 and Co1–Co3 would form an idealized angle of 90° to the Co_3 plane in **2**. In **5**, they bend back to 119.4°, presumably to minimize steric interactions between the cyclohexyl groups and the carbonyl groups. There are two motions associated with the $Co(CO)_2$ groups at Co2 and Co3. First, the carbonyls that lie in the Co_3 plane in **2** bend toward the in-plane bridging phosphido group to preserve octahedral coordination. The C4–Co2–P2 and C6–Co3–P2 angles are 97.0 (5) and 97.1 (6)°, respectively. Second, each $Co(CO)_2$ group rocks in a direction *toward* the adjacent, out-of-plane bridging phosphido group. Thus, with reference to Figure 2, the C3–Co2 vector makes a 101.6° angle with the Co_3 plane. Likewise, the C4–Co2 vector is bent 22.4° out of the Co_3 plane. This rocking motion is again an attempt to preserve octahedral coordination at Co2 and Co3. The rather complicated experimental structure can, therefore, be traced rather easily back to the $M_3(CO)_{12}$ prototype.

An alternative substitution pattern in $M_3(CO)_{12}$ would be to replace all carbonyl groups that lie in the M_3 plane by phosphido groups, giving structure **3** in Scheme I. The remaining carbonyl groups will then bend toward each other to give **6**. Perhaps the easiest way to view this distortion is to consider each $M(CO)_4$ unit as a trigonal bipyramid. Replacing the six equatorial carbonyls by three bridging phosphido groups geometrically requires them to be diaxial. The remaining carbonyls complete this Berry pseudorotation sequence by assuming diequatorial positions. The symmetry of the resultant structure can remain D_{3h}. The third possible isomer is one where four equatorial carbonyls are replaced by two in-plane phosphido groups and two axial carbonyls (at Co1 and Co2 in **4**) are replaced by an out-of-plane phosphido group. The remaining carbonyls at Co3 complete the Berry pseudorotation sequence by moving toward each other, and those at Co1 and Co2 distort, in a way analogous to what occurs at Co2 and Co3 in **5**, to give **7**, which has C_s symmetry.

A central issue in this work is the dynamics of phosphido bridge interconversions. Does either the D_{3h} isomer (**6**) or the C_s structure (**7**) serve as a transition state (or intermediate) for the low-energy fluxional process observed in solution? We think not. Extended Hückel calculations were carried out on **5**–**7** for $[Co(\mu\text{-}PH_2)(CO)_2]_3$. Computational and geometric details are given in the Experimental Section. The experimentally observed C_2 structure (**5**) was found to be the ground state, while the D_{3h} (**6**) and C_s (**7**) structures were 67 and 24 kcal/mol, respectively, higher in energy.

There are two useful ways to explain the very high energies associated with the D_{3h} and C_s isomers. First of all, let us remove the specific geometrical and electronic factors that are created by the bridging phosphido groups by replacing each with two σ-donor ligands. The classic M_3L_{12} structure shown at the top of Figure 3a is then a model for the C_2 isomer. Its bonding, which has been treated elsewhere,[10] can be conveniently constructed by interacting three d^8 ML_4 units. Each ML_4 unit possesses three low-lying orbitals.[11] These interact with each other to a minor

(10) (a) Schilling, B. E. R.; Hoffmann, R. *J. Am. Chem. Soc.* **1979**, *101*, 3456. (b) Evans, D. G.; Mingos, D. M. P. *Organometallics* **1983**, *2*, 435. (c) Green, J. C.; Seddon, E. A.; Mingos, D. M. P. *J. Chem. Soc., Chem. Commun.* **1979**, 941; *Inorg. Chem.* **1981**, *20*, 2595. (d) Sherwood, D. E.; Hall, M. B. *Ibid.* **1982**, *21*, 3458. (e) Tyler, D. R.; Levenson, R. A.; Gray, H. B. *J. Am. Chem. Soc.* **1978**, *100*, 7888. (f) Korol'kov, D. V.; Meissner, H. *Z. Phys. Chem. (Leipzig)* **1973**, *253*, 25. (g) Related M_3L_n clusters have been studied by: Mealli, C. *J. Am. Chem. Soc.* **1985**, *107*, 2245. Underwood, D. J.; Hoffmann, R.; Tatsumi, K.; Nakamura, A.; Yamamoto, Y. *Ibid.* **1985**, *107*, 5968. Dedieu, A.; Hoffmann, R. *Ibid.* **1978**, *100*, 2074. Hofmann, P.; Rösch, N.; Schmidt, H. R. *Inorg. Chem.* **1986**, *25*, 4470. Evans, D. G.; Mingos, D. M. P. *J. Organomet. Chem.* **1982**, *240*, 321. Braunstein, P.; Rose, J.; Dedieu, A.; Dusausoy, Y.; Mangeot, J.-P.; Tiripicchio, A.; Tiripicchio-Camellini, M. *J. Chem. Soc., Dalton Trans.* **1986**, 225.

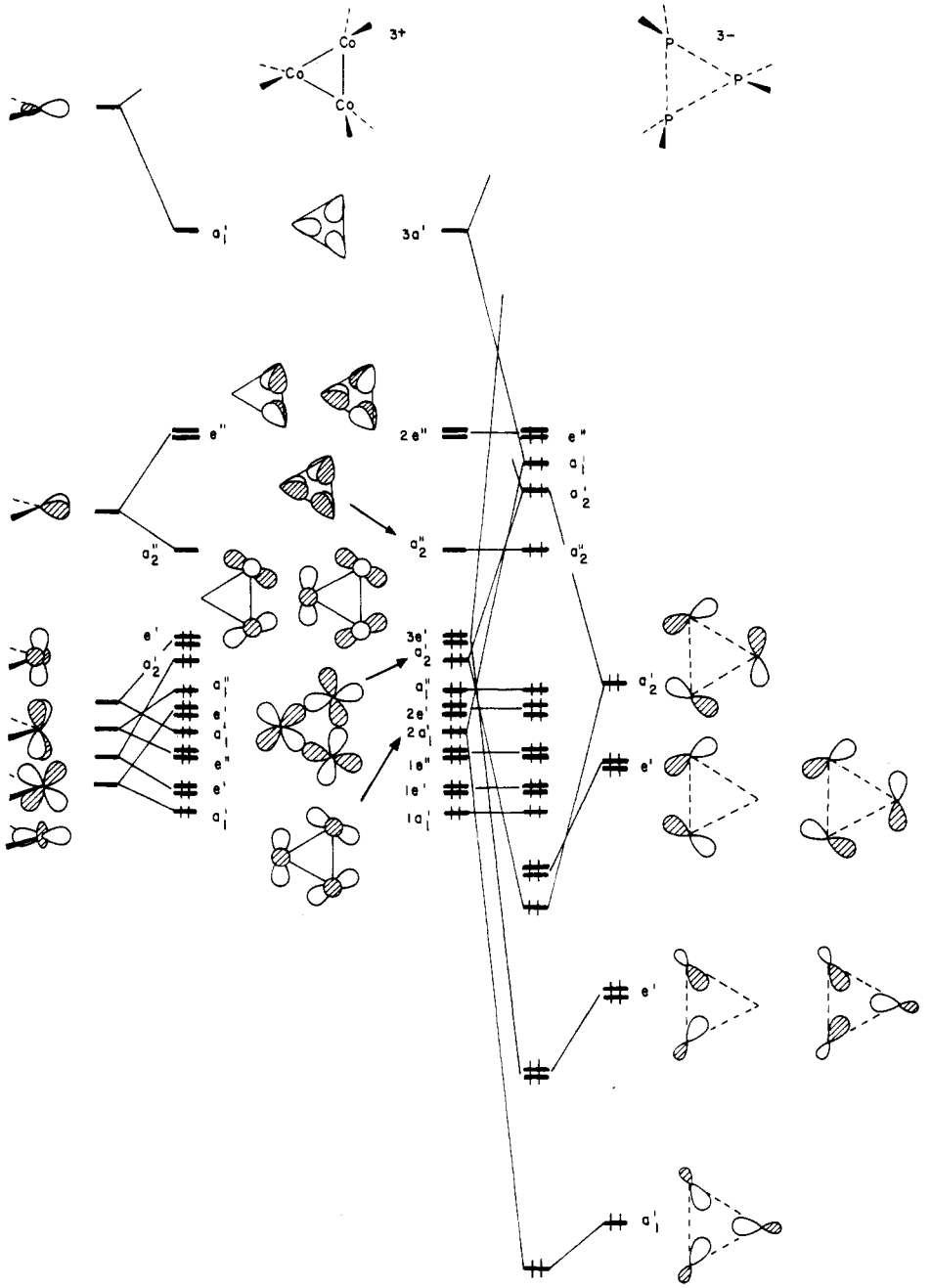

Figure 4. Construction of the valence orbitals of $[Co(CO)_2(\mu\text{-}PH_2)]_3$ at D_{3h} symmetry.

extent and form a block of nine occupied, corelike orbitals. At higher energy, each ML_4 group uses a hybrized a_1 and b_2 orbital for M–M bonding. These are shown on the left side of Figure 3a. The b_2 orbitals combine to form two bonding (1e′) and one antibonding (a_2') molecular orbitals. The a_1 orbitals form a bonding (a_1') and two antibonding (2e′) levels. There are a total of six electrons that fill 1e′ + a_1'. These three occupied molecular orbitals are nothing more than the symmetry-adapted linear combinations of the three M–M σ orbitals. To be sure, there will be intermixing between the 1e′ and 2e′ sets, as there is in the Walsh model for cyclopropane and isolobal molecules.[11a,12] Specifically, 2e′ will mix into 1e′ in a bonding way to further stabilize the latter. The model for the D_{3h} isomer is illustrated in Figure 3b. The three a_1 functions split in the same way (and to the same extent) as before. The b_2 orbitals, however, now have π-type overlap and yield one bonding (a_2'') and two antibonding (c″) orbitals. For simplicity, we have used a splitting identical with that in Figure 3a. The important point is that now the antibonding e″ set *must* be half-filled. Clearly, the bonding situation illustrated in Figure 3b is much less stable than that associated with Figure 3a. The pattern for a model of the C_s isomer is also easily constructed, as shown in Figure 3c. The pattern of three orbitals derived from the a_1 hybrids is again, to a first approximation, unaltered. The three b_2 functions now produce one bonding ($1a_1$), one nonbonding (b_2), and one antibonding ($1b_1$) molecular orbital. Thus, Figure 3c represents a situation intermediate between those found in Figure 3a,b. This is exactly what is predicted by the relative energy difference for $[Co(\mu\text{-}PH_2)(CO)_2]_3$. This analysis is, of course, very idealized, and it totally neglects the special properties that the bridging phosphido groups bring to the structure.

A more detailed way to understand the relative energies associated with the three isomers is to derive the orbitals for the high-symmetry D_{3h} system. The energy changes of selected valence orbitals are then examined with respect to deformation to the C_2

(11) (a) Albright, T. A.; Burdett, J. K.; Whangbo, M.-H. *Orbital Interactions in Chemistry*; Wiley: New York, 1985. (b) Elian, M.; Hoffmann, R. *Inorg. Chem.* **1975**, *14*, 1058. (c) Burdett, J. K. *J. Chem. Soc., Faraday Trans. 2* **1974**, *70*, 1599.

(12) (a) Schoeller, W. W.; Dabisch, T. *Inorg. Chem.* **1987**, *26*, 1081. (b) Honegger, E.; Heilbronner, E.; Schmelzer, A. *Nouv. J. Chim.* **1982**, *6*, 519. (c) Jorgensen, W. L.; Salem, L. *The Organic Chemist's Book of Orbitals*; Academic: New York, 1973.

or C_s structure. Figure 4 shows the building-block process for constructing the valence orbitals of $[Co(\mu\text{-}PH_2)(CO)_2]_3$ at the D_{3h} geometry. The phosphido group can be considered a four-electron donor; symmetry-adapted combinations of the two lone-pair orbitals generate **8** and **9**.[10g,11a] Three "radial" (**8**) lone

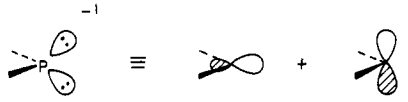

8 **9**

pairs for the $(PH_2)_3^{3-}$ fragment yield fragment orbitals of a_1' and e' symmetries, while combination of the three "tangential" (**9**) lone pairs gives fragment orbitals of e' and a_2' symmetries. These six delocalized combinations are shown on the right side of Figure 4. The orbitals of a d^8 $Co(CO)_2^+$ monomer[11a] are explicitly shown on the far left side of Figure 4. These split in a straightforward manner to give the $[Co(CO)_2]_3^{2+}$ fragment orbitals. For clarity purposes, two combinations of cobalt-centered 4p orbitals, **10** and **11**, are not shown but do figure into our discussion. The two e'

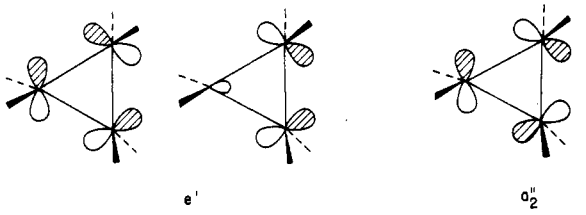

10 **11**

sets of $(PH_2)_3^{3-}$ combine with 3e' and **10** to give two filled bonding and two empty antibonding molecular orbitals. The a_1' phosphido trimer level interacts with $2a_1'$ *and* $3a_1'$. Bonding, nonbonding, and antibonding molecular orbitals are produced. Notice that the bonding and nonbonding levels are filled. This latter orbital is kept at low energy because while a_1' mixes into $2a_1'$ in an antibonding fashion (**12**), a significant amount of $3a_1'$ (49%) mixes

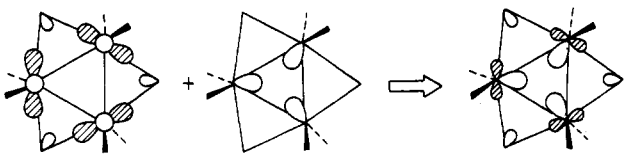

12 **13**

into this level in a bonding way with respect to a_1', producing **13**. The a_2' fragment orbital on the phosphido trimer interacts with a_2' and **11** to produce another three-orbital pattern of bonding, nonbonding, and antibonding molecular orbitals. Again, the bonding and nonbonding levels are filled. All other fragment orbitals in the $[Co(CO)_2]_3^{3+}$ fragment are essentially nonbonding with respect to $(PH_2)_3^{3-}$. Note in particular the presence of three Co–Co π levels, a_2'' and e''; the latter is half-filled. The relationship between the molecular orbitals of D_{3h} $[Co(\mu\text{-}PH_2)(CO)_2]_3$ and the simplified bonding model in Figure 3b is clear. Molecular a_2'' and e'' in Figure 4 are precisely analogous to a_2'' and e'' in Figure 3b. Furthermore, **13** is topologically identical with a_1' in Figure 3b. The D_{3h} isomer with two electrons in e'' is Jahn–Teller unstable. According to the McIver–Stanton rules,[13] it *cannot* serve as a transition state for the interconversion of C_2 isomers.

We now proceed to analyze the distortion from the D_{3h} structure to a C_2 isomer. An orbital correlation diagram for the most important molecular orbitals is shown in Figure 5. There are basically three motions that describe this distortion. The two phosphido groups that bridge Co1–Co2 and Co1–Co3 move in front of and behind the plane of the paper, respectively. The $Co(CO)_2$ unit at Co2 as a whole rocks into the plane of the paper, while that at Co3 rocks in front of the plane, as shown by the arrows for the structure at the top of Figure 5. Finally, the

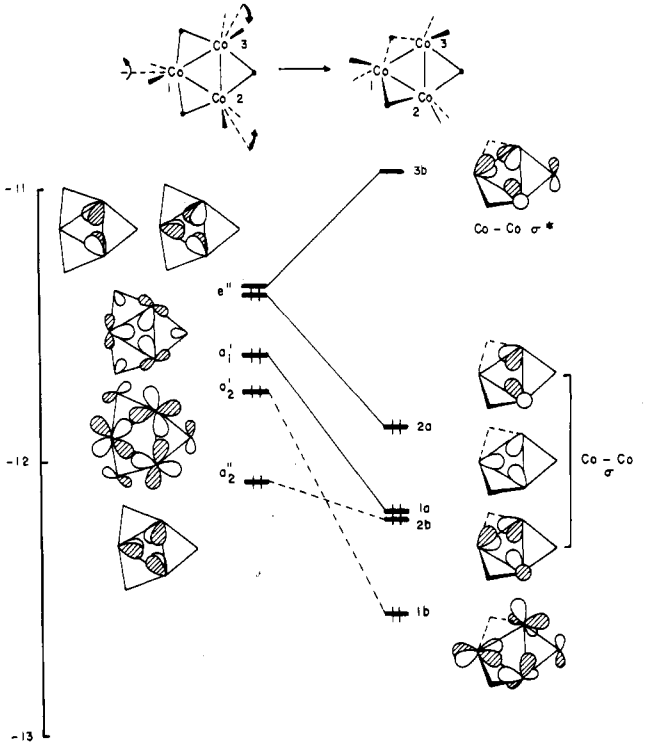

Figure 5. Orbital correlation diagram for the D_{3h} to C_2 distortion. The a_2' to 1b and a_2'' to 2b orbitals will actually undergo an avoided crossing along this distortion path.

$Co(CO)_2$ unit at Co1 rotates in a clockwise direction. Let us start the discussion with the lower member of the e'' set on the left side of Figure 5. The rocking motion at Co2 and Co3 brings the shaded lobes into the Co_3 plane. A π-antibonding orbital is turned into a Co2–Co3 σ-bonding one. Consequently, this component of e'' is stabilized. In the other component of e'', the rocking motion at Co2 brings the shaded lobe and the unshaded one at Co3 into the Co_3 plane. The twisting motion at Co1 also turns on a σ-antibonding interaction with these two lobes. Thus, this component of e'' is destabilized and a significant HOMO–LUMO gap is introduced. The a_1' orbital is stabilized upon distortion, principally because the phosphido groups between Co1–Co2 and Co1–Co3 move into nodal planes. This factor also serves to stabilize the a_2' level; furthermore, the rocking and twisting motion of the $Co(CO)_2$ units reduce Co–Co σ antibonding. Finally, the a_2'' orbital is not much affected. Co2–Co3 σ antibonding is introduced while Co1–Co2 and Co1–Co3 σ bonding is turned on. The 2a and 2b molecular orbitals in the C_2 structure are topologically analogous to the 1e' set in Figure 3a, and 1a is identical with a_1'. This D_{3h} to C_2 distortion then converts one π and one π^* Co–Co orbital into two Co–Co σ bonds. Moreover, antibonding with the bridging phosphido lone pairs is largely removed. These factors produce the 67 kcal/mol stabilization of the C_2 ground state over the D_{3h} structure. Putting this another way, any structure close to D_{3h} is expected to be energetically nonviable as a transition state for the fluxionality observed in $[Co(\mu\text{-}PR_2)(CO)_2]_3$.

Distortion from D_{3h} to a C_s geometry (see **7**, Scheme I) is also stabilizing. In this case the rocking motion at Co2 and Co3 proceeds in the same direction (see Figure 5), and the phosphido bridge between these two cobalt atoms moves out of the Co3 plane in the opposite direction. Now the lower component of e'' in Figure 5 will be destabilized, yielding a Co–Co σ^* orbital. The upper component of e'' and a_2'' will mix with each other to produce a Co2–Co3 σ bonding and a *nonbonding* one localized on Co1 (analogous to the b_2 orbital in Figure 3c). The a_1' and a_2' levels will not be stabilized as much as that shown in Figure 5 since one phosphido group (rather than two) moves out of the Co_3 plane. Consequently, the C_s structure is higher in energy than the C_2 one. The 24 kcal/mol energy difference may not be accurate given the crude nature of the extended Hückel method and the geo-

(13) McIver, J. W.; Stanton, R. E. *J. Am. Chem. Soc.* **1972**, *94*, 8618.

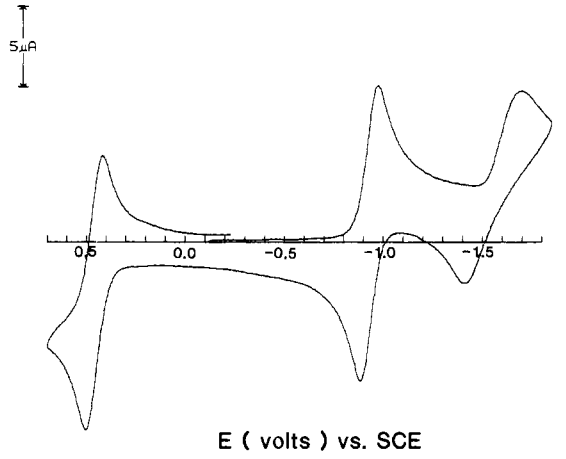

Figure 6. Cyclic voltammogram of **1** at 200 mV/s with *iR* compensation.

metrical constraints we have employed; however, our analysis shows that it must be sizable, at least the amount of energy required to convert a Co–Co σ orbital into a nonbonding one. We propose that an energetically less costly process for the interconversion of C_2 isomers occurs via the motions shown in **14**. One

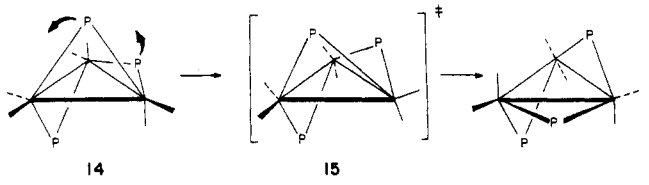

out-of-plane and the in-plane phosphido groups simultaneously move to yield **15**, where all three phosphido groups lie out of the Co_3 plane. **15** can maximally have C_s symmetry and will have one largely nonbonding orbital at high energy analogous to **7**. However, this will be greatly compensated by the removal of lone-pair repulsions from the phosphido groups. But there is no reason to suppose that the transition state must have C_s symmetry. The two phosphido groups need not move at the same rate, and the structure[7] of $[Co(\mu\text{-}PMe_2)(CO)_2]_3$ suggests that this is likely to be the case. Searching for a transition state with this many degrees of freedom is currently beyond our capabilities. It may be possible to chart the reaction path by X-ray structures of derivatives where the steric bulk of the alkyl substituents on the phosphido groups is varied. We shall explore this possibility in the future.

Electrochemical Studies. Cyclic voltammetry (CV) of **1** shows three waves (Figure 6). Oxidation of **1** occurs in a Nernstian wave at 0.49 V vs SCE. The separation of peak potentials, ΔE_p, is near the expected 59 mV at a scan rate, v, of 20 mV s^{-1}. Although *iR* compensation through positive feedback was employed, some uncompensated resistive effects in the resistive THF solution were found a higher scan rates where larger currents flowed. Thus, for the oxidation wave, the ratio of cathodic (reversal) to anodic peak currents (i_{pc}/i_{pa}) was nearly 1, and a plot of i_{pa} vs $v^{1/2}$ was linear and intercepted the origin for v between 20 and 1000 mV s^{-1}. Above 1 V s^{-1} some deviation from the i_{pa}–$v^{1/2}$ line was observed, probably because of uncompensated resistive effects. **1** also undergoes a Nernstian reduction at −0.96 V vs SCE. The wave shape parameters and behavior are essentially the same as those for the oxidation wave. In both cases, the number of Faradays/mol of **1** passed during the bulk electrolysis, n_{app}, was 0.95 ± 0.05. Exhaustive electrolysis to form the radical anion results in the formation of a green solution that exhibits an ESR signal (Figure 7). The signal is quite broad, presumably because of coupling to three cobalt atoms and the in-plane phosphorus. Our calculations indicate the singly occupied orbital (3b in Figure 5) to be 36% on Co1, 34% on Co2, and 7% on the phosphorus atom that bridges Co2–Co3.

A second reduction wave, ascribed to reduction of the radical anion to a dianion, occurs at −1.56 V vs SCE. This wave shows

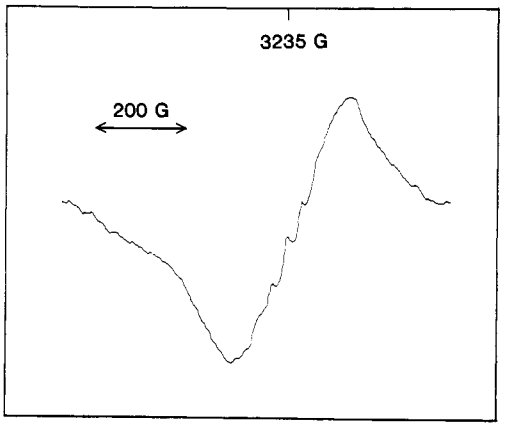

Figure 7. X-Band ESR spectrum of the radical anion of **1**.

a $\Delta E_p > 59$ mV that increases with increasing v (at scan rates where ΔE_p for the other waves is near 59 mV, indicating that the increased peak splitting is not attributable to uncompensated resistance effects). Bulk electrolysis at this wave occurs with $n_{app} \sim 1$ and produces a red solution that exhibits an ESR signal with either $g = 4$ or $g = 2$. CV of the reduced solution shows an oxidation wave at the same potential as the first reduction wave in the solution of **1**, for oxidation of dianion to radical anion. Bulk electrolysis at this oxidation wave quantitatively regenerates **1**, showing that the dianion is stable (in the absence of air or moisture) and that no follow-up reactions of the dianion occur on either the cyclic voltammetric or coulometric time scale. The heterogeneous-electron-transfer rate constant for the reduction of the anion radical to the dianion, k^0, was estimated as $\sim 10^{-4}$ cm s^{-1} by comparing i_{pc} for this wave to that for the first Nernstian reduction.[14] The quasi-reversibility of this wave suggests significant structural changes upon reduction of the radical anion to the dianion, as opposed to reduction of **1** to the radical anion.

Both the radical anion and the dianion are stable in the absence of air or moisture. Exposure of either to air, moisture, halogenated hydrocarbons, or any potential electron acceptor regenerates the neutral species **1**, indicating that both the radical anion and dianion are chemically reversible, outer-sphere electron donors. Placing two electrons in the 3b orbital (see Figure 5) should elongate particularly the Co1–Co2 and Co1–Co3 bonds. Our calculations predict that when these two bonds are lengthened by 0.11 Å, the C_2 structure is stabilized by 5 kcal/mol. The D_{3h} and C_s structures remain at higher energies for the dianion (50 and 12 kcal/mol, respectively, higher in energy). One can see in Figure 5 that although the 3b level is greatly stabilized on going to the D_{3h} structure, the 1b, 1a, and 2a orbitals are destabilized.

Conclusions

We have described the synthesis, structure, and electrochemistry and related computations for the Co_3 cluster $[Co(\mu\text{-}Cy_2P)(CO)_2]_3$. Extended Hückel calculations have been of help in understanding the possible modes of interconversion of different geometries of the molecule in solution. Further studies are in progress.

Experimental Section

All manipulations were performed under nitrogen or vacuum. Microanalyses were performed by the Schwarzkopf Microanalytical Laboratory, Woodside, NY. Toluene was dried over, and then distilled from, sodium under nitrogen before use. Melting point determinations were carried out in sealed tubes, under 1 atm of N_2, and are uncorrected. Cy_2PH was purchased from Strem Chemicals, Inc., and stored under nitrogen. $Co_2(CO)_8$ was purchased from Strem Chemicals, Inc., and stored under CO at −20 °C. Infrared spectra were run on a Perkin-Elmer 1330 spectrometer and calibrated against a polystyrene standard. NMR spectra were run on Nicolet NT-500 (^{13}C, 125.77 MHz), Nicolet NT-200 (^{31}P, 81.01 MHz), Bruker WH-90 (^{31}P, 36.43 MHz), Varian FT-80 (^{31}P, 35.45 MHz), and Varian EM-390 (^1H, 90 MHz) spectrometers. For ^1H NMR spectra, samples were run at ambient temperature and referenced

(14) Bard, A. J.; Faulkner, L. R. *Electrochemical Methods*; Wiley: New York, 1980; pp 224–227.

to external Me_4Si (δ 0.0). For ^{31}P NMR spectra, samples were run at both ambient and variable temperatures (see Results and Discussion) and were referenced to external 85% H_3PO_4 (δ 0.0; positive is downfield). The electron spin resonance (ESR) measurements were carried out with a Varian E-9 X-band spectrometer at room temperature with modulation amplitude = 8.0 G, microwave frequency = 9.308 GHz, and microwave power = 80 mW.

$[Co(\mu\text{-}Cy_2P)(CO)_2]_3$ (1). Dicyclohexylphosphine (1.91 mL, 8.78 mmol) was added dropwise to a solution of $Co_2(CO)_8$ (1.50 g, 4.39 mmol) in toluene (100 mL) at 0 °C. The red-brown solution was allowed to warm to room temperature (0.5 h) and then refluxed overnight (ca. 8 h). The green solution was allowed to cool to room temperature, and volatile materials were removed under vacuum. The dark green residue was extracted with toluene (2 × 20 mL), yielding a dark green solution, which was filtered and evaporated to ca. 20 mL under vacuum. Cooling (−20 °C) yielded dark green crystals after ca. 72 h. The crystals were collected and dried under vacuum at room temperature. The compound is air stable in solution and in the solid state. The procedure can be successfully scaled up to use ca. 5 g of $Co_2(CO)_8$. Yield: 1.74 g, 65%. Mp: 204–208 °C dec. IR (hexane solution, CaF_2 cells): 2005 s, 1970 s, 1955 s, 1930 s cm^{-1}. IR (Nujol mull, CsI plates): 2005 s, 1970 s, 1945 s, 1930 s, 1345 w, br, 1290 w, 1260 m, 1185 w, 1165 m, 1110 w, 995 w, 880 m, 845 m, 805 m, br, 735 w, 725 w, 550 w, 520 s, 405 m, br cm^{-1}. ^1H NMR (C_6D_6): δ 2.38 br m, 2.08 s, 1.62 br m, 1.18 br m ($(C_6H_{11})_2P$). $^{13}C\{^1H\}$ NMR (C_6D_6): δ 209.7 br s ($\Delta w_{1/2}$ = 29 Hz, *C*O), 48.9 s, 33.8 s, 27.9 s, 26.3 s (C_6H_{11}). $^{31}P\{^1H\}$ NMR (C_6D_6): δ 319.20 br s ($\Delta w_{1/2}$ = 80.6 Hz).

X-ray Crystallography. Crystals suitable for X-ray diffraction were grown by slow cooling of a concentrated toluene solution (−20 °C). The crystals were mounted in thin-walled glass capillaries and sealed under vacuum. Data are shown in Table I.

Unit cell parameters were obtained by carefully centering 25 strong reflections having 2θ values between 26 and 28°. The space group $P2_1/a$ was uniquely determined by the systematic absences $h0l$ ($h = 2n + 1$) and $0k0$ ($k = 2n + 1$). Data were collected in the $+h,+k,\pm l$ quadrant between 2θ values of 2 and 50° on an Enraf-Nonius CAD-4 diffractometer. The data were then corrected for Lorentz and polarization effects. The check reflections showed a 1% decrease in intensity over the course of data collection, and hence, no correction was applied. A ψ scan of four reflections having χ values between 80 and 90° showed a minimum transmission of 83.3% and a maximum transmission of 99.9%. An empirical absorption correction was applied (program EAC). The observed structure factors of equivalent reflections were averaged, with agreement factors of 0.052 on intensity and 0.050 on F_o. The positions of the heavy atoms were obtained by direct methods (MULTAN),[15] and the remaining non-hydrogen atoms were located by successive cycles of different Fourier maps followed by least-squares refinement. Hydrogen atoms were not located. Data with intensities less than $3\sigma(I)$ and with $(\sin\theta)/\lambda$ less than 0.05 $Å^{-1}$ were excluded, and a non-Poisson contribution weighting scheme with an instability factor P set at 0.06 was used in the final stages of refinement.[16] The structure was refined to the final values shown in Table I. The maximum peak in the final difference Fourier map had a height of 0.611 e/$Å^3$. Scattering factors were taken from ref 17. Supplementary material is available.[18]

Electrochemistry. All electrochemical measurements were performed in a conventional three-electrode cell by using a Princeton Applied Research (PAR) Model 173 potentiostat, PAR Model 175 universal programmer, PAR Model 179 digital coulometer (Princeton Applied Research Corp., Princeton, NJ), and a Model 2000 X-Y recorder (Houston Instruments, Inc., Austin, TX). The voltammograms were obtained with a platinum-disk electrode (area 0.018 cm^2) whereas bulk electrolyses were carried out with a platinum-gauze electrode (area 10 cm^2). The surface of the platinum disk was checked for cleanliness by running cyclic voltammograms in 1.0 M H_2SO_4. Positive feedback was used to compensate for iR drop. The reference electrode was a silver wire (quasi-reference electrode). The silver wire was cleaned the same way (dilute HNO_3, deionized H_2O) each time to give a constant potential. Ferrocene was added to the solutions at the end of each experiment in order to reference the voltammetric waves to SCE. The solvent employed was THF, which was first purified by distillation from NaK alloy. Before use, the solvent was vacuum-distilled from Na/benzophenone into the cell on a high-vacuum line. The electrolyte, tetrabutylammonium tetrafluoroborate, was twice recrystallized from ethyl acetate/diethyl ether and dried under vacuum (10^{-5} Torr, 140 °C) before use. Background voltammograms were run to verify the purity of the system as evidenced by the reduction of the solvent at the theoretical limit (−3.0 V vs SCE).

Molecular Orbital Calculations. Molecular orbital calculations at the extended Hückel level[19] used the modified Wolfsberg–Helmholz formula.[20] Orbital exponents and H_{ii}'s were taken from previous work.[21] The geometrical parameters for the C_2 structure of $[Co(\mu\text{-}PH_2)(CO)_2]_3$ were taken from the experimental structure of **1** with P–H lengths of 1.41 Å and H–P–H angles of 106.0°. In the D_{3h} structure, the Co–Co lengths were 2.573 Å and the C–Co–C angles were 100.0°. In the C_s structure, the two Co–Co bonds bridged by the in-plane phosphido groups were elongated to 2.685 Å and the out-of-plane phosphido group formed a dihedral angle of 60.6° to the Co_3 plane.

Acknowledgments. We thank the National Science Foundation (Grants CHE-8517759 and CHE-8402135), the Robert A. Welch Foundation (Grants F-816 and E-705), the Texas Advanced Technology Research Program, and the donors of the Petroleum Research Fund, administered by the American Chemical Society, for support. R.A.J. also thanks the Alfred P. Sloan Foundation for a fellowship (1985–1987).

Registry No. **1**, 112896-20-5; $Co_2(CO)_8$, 15226-74-1; $[Co(\mu\text{-}PH_2)(CO)_2]_3$, 112896-21-6.

Supplementary Material Available: Complete tables of bond lengths and angles and temperature factors for **1** (8 pages); complete tables of observed and calculated structure factors for **1** (38 pages). Ordering information is given on any current masthead page.

(15) Germain, G.; Main, P.; Wolfson, M. M. *Acta Crystallogr., Sect. A: Cryst. Phys., Diffr., Theor. Gen. Crystallogr.* **1971**, *A27*, 368. All calculations were performed on a PDP 11/44 computer using the SDP-PLUS software package (B. A. Frenz and Associates, College Station, TX, 1981).

(16) P is used in the calculation of $\sigma(I)$ to downweight intense reflections in the least-squares refinement. The function minimized was $\sum w(|F_o| - |F_c|)^2$, where $w = 4(F_o)^2/[\sum(F_o)^2]^2$, $[\sum(F_o)^2]^2 = [S^2(C + R^2B) + (P(F_o)^2)^2]/Lp^2$, S is the scan rate, C is the total integrated peak count, R is the ratio of scan time to background counting time, B is the total background count, and Lp is the Lorentz–Polarization factor. The magnitude of P = 0.06 indicates there may be nonlinearity in the counting chain.

(17) *International Tables for X-ray Crystallography*; Kynoch: Birmingham, England, 1974; Vol. 4.

(18) See paragraph at end of paper regarding supplementary material.

(19) Hoffmann, R. *J. Chem. Phys.* **1963**, *39*, 1397. Homann, R.; Lipscomb, W. N. *Ibid.* **1962**, *36*, 2179; **1962**, *37*, 2872.

(20) Ammeter, J. H.; Bürgi, H.-B.; Thibeault, J. C.; Hoffmann, R. *J. Am. Chem. Soc.* **1978**, *100*, 3686.

(21) Albright, T. A.; Hofmann, P.; Hoffmann, R. *J. Am. Chem. Soc.* **1977**, *99*, 7546.